A. Chiarini, M. Quadrio, F. Auteri
A New Scaling for the Flow Instability Past Symmetric Bluff Bodies
Journal of Fluid Mechanics, Vol. 936, R2, 2022, R2 (11 pages)
doi:10.1017/jfm.2022.99

A new scaling for the steady flow past two-dimensional bluff bodies

A. Chiarini[1], M. Quadrio[1] and F. Auteri[1]

[1]Dipartimento di Scienze e Tecnologie Aerospaziali, Politecnico di Milano, via La Masa 34, 20156 Milano, Italy

(Received xx; revised xx; accepted xx)

A scaling law to predict the onset of the primary Hopf instability in the steady flow past two-dimensional, symmetric bluff bodies is proposed. It uses a measure of the spatial extent of the separation bubble as length scale and the largest reverse-flow speed within it as velocity scale. The ensuing Reynolds number, evaluated at the onset of the primary Hopf bifurcation, collapses quite nicely for bodies of different shape and aspect ratio even when a small angle of attack perturbs the symmetry; its relative variation is one order of magnitude smaller than that of the usual Reynolds number defined with the free-stream velocity and the cross-stream body size. With the new scaling, it can be roughly assessed whether the steady flow past a two-dimensional bluff body is absolutely and globally unstable to two-dimensional perturbations without a computationally expensive stability analysis: only the inspection of the base flow is required. More importantly, the scaling provides an insight into the flow mechanism that produces the instability.

Key words:

1. Introduction

The nature of the incompressible flow past a two-dimensional symmetric bluff body changes with the Reynolds number, and ranges from a symmetric steady state to the chaotic and unsteady turbulent regime, depending on the relative importance of inertial and viscous forces. A complete description of the flow, therefore, includes the knowledge of the critical Reynolds numbers at which the flow changes regime, i.e. the Reynolds number corresponding to the first onset of the several instabilities the flow undergoes. For this type of flows, the Reynolds number usually employed is based on the body thickness D and on the free-stream velocity U_∞ as length and velocity scales, and is thus defined as $Re = U_\infty D/\nu$, where ν is the kinematic viscosity. These scales, however, could not always be best suited to describe the physics of the problem at hand, and alternative choices might be more appropriate to predict the onset of a new regime. deally, one

would want the critical value of the associated Reynolds number to be the same for bodies with different cross-sectional shape, as long as the physics remains the same.

When the Reynolds number is large enough, the flow past a symmetric two-dimensional bluff body undergoes a first two-dimensional instability — known as primary instability — which usually corresponds to a Hopf bifurcation from the symmetric steady state towards a time-periodic non-symmetric state characterised by vortex shedding (Provansal *et al.* 1987; Monkewitz *et al.* 1993; Noack & Eckelmann 1994). While the instability mechanism is ostensibly the same for bodies of different shape, the critical Reynolds number Re_c bears a significant dependence on the geometry and flow configuration. Several numerical studies and experiments found that, for a circular cylinder, the onset of the primary instability occurs at $Re = Re_c \approx 47$ (Giannetti & Luchini 2007; Marquet *et al.* 2008; Williamson 1996). Jackson (1987) studied the onset of the primary instability for ellipses, flat plates and triangles varying the aspect ratio $\mathit{Æ} = L/D$, where L and D are the streamwise and maximum cross-stream dimensions of the bodies, and the incidence angle. He reported $Re_c \approx 27.7$ for a normal flat plate, $Re_c \approx 76.7$ for an ellipse parallel to the incoming flow with $\mathit{Æ} = 2$, and $Re_c \approx 36$ for an equilateral triangle oriented towards the flow. For all these geometries, a large increase of Re_c with $\mathit{Æ}$ was observed. Thompson *et al.* (2014) studied the wake past elliptic cylinders ranging from a normal flat plate to the circular cylinder, finding a monotonic increase of Re_c, from $Re_c \approx 31.6$ to $Re_c \approx 47.2$. Park & Yang (2016) determined how the primary instability is affected by rounding the four corners of a square cylinder, exploring shapes between the square cylinder with sharp edges and the circular cylinder. The onset of the primary instability was found to change non-monotonically with the corner curvature; the most stable configuration is intermediate between the circular and square cylinders and has $Re_c \approx 47.3$. More recently, we have studied the primary instability of the flow past rectangular cylinders by varying the aspect ratio in the range $0.25 \leqslant \mathit{Æ} \leqslant 30$, and by rounding the leading-edge and/or trailing-edge corners (Chiarini *et al.* 2021*a*). Results indicated that Re_c increases monotonically with $\mathit{Æ}$ from $Re_c \approx 34.2$ to $Re_c \approx 140$; its dependence on the corner curvature is non-monotonic and changes with $\mathit{Æ}$.

The large variability of Re_c suggests that D and U_∞ might not be the most appropriate length and velocity scales to describe the primary Hopf bifurcation and to predict its onset. In fact, in Chiarini *et al.* (2021*a*) we have shown that the length of the separation bubble in the wake and the largest reverse-flow speed measured in it are more suitable scales, for rectangular cylinders: the former dictates the spatial extent of the absolute instability pocket (Chomaz 2005), while the latter directly impacts the local amplification of the unstable wave packets (Hammond & Redekopp 1997). For rectangular cylinders, the associated Reynolds number evaluated at criticality was found to be (nearly) independent on the aspect ratio and its variation to be one order of magnitude lower than that of the conventional Reynolds number based on D and U_∞. After all, the body thickness D is not always the proper length scale to describe the flow past bluff bodies also at larger Reynolds numbers. For example, Mat Ali *et al.* (2011) observed that the half-width wake thickness (Pope 2000) is more appropriate for predicting the Strouhal number of the unsteady flow past a square cylinder with a splitter plate. In contrast, several authors observed that the cylinder length L is the proper length scale for describing the periodic flow past elongated rectangular

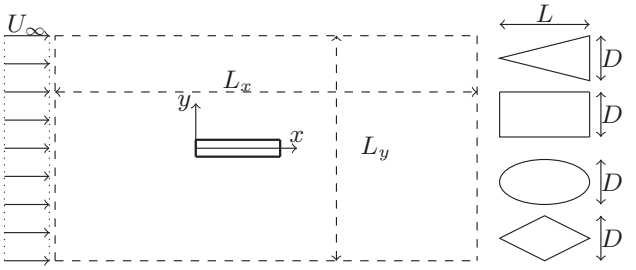

Figure 1: Sketch of the computational domain with the geometry of the triangular, rectangular, elliptical and diamond cylinders.

cylinders at intermediate Reynolds numbers (see for example Okajima 1982; Chiarini *et al.* 2021*b*) and that the Strouhal number based on it has an almost stepwise dependence on AR due to the interaction of the impinging-shear-layer instability with the trailing-edge vortex shedding (Hourigan *et al.* 2001).

In this work, we assess the generality of the scaling presented in Chiarini *et al.* (2021*a*) for the primary Hopf bifurcation, by considering four different geometries (triangle, rectangle, ellipse and diamond), that yield a steady base flow with different features due to the different placement of the corners (or lack thereof). For each geometry the aspect ratio is varied in the range $1 \leqslant \mathit{AR} \leqslant 8$. We also show that the new scaling works pretty well for small asymmetries of the flow and when other wake-related length scales are used, provided that they are a measure of the spatial extent of the separation bubble. The work is organised as follows. After this introduction, the numerical approach is described in §2. The results are presented in §3 and the validity of the proposed scaling is addressed in §4. Finally, some concluding remarks are drawn is §5.

2. Methods

The incompressible flow over two-dimensional cylinders of different cross-sectional shape with aspect ratio $1 \leqslant \mathit{AR} \leqslant 8$ is considered. Figure 1 shows the geometries and the notation. A Cartesian coordinate system with origin placed at the leading edge of the cylinders is used, with the x and y axes denoting the streamwise and vertical directions, respectively. The cylinders have length L and maximum thickness D and are placed in a uniform flow with velocity U_∞ with their symmetry axis aligned with the free-stream velocity. The computational domain extends for $-25 \leqslant x/D \leqslant 75$ and $-40 \leqslant y/D \leqslant 40$ in the two directions corresponding to $L_x = 100D$ and $L_y = 80D$; it has been shown (Chiarini *et al.* 2021*a*) that these dimensions are adequate to investigate the onset of the primary instability of the flow past bluff bodies with aspect ratio up to $\mathit{AR} = 30$. The Reynolds number is based on U_∞ and D and is thus defined as $Re = U_\infty D/\nu$.

To obtain the base flow, the two-dimensional version of the steady Navier–Stokes equations is solved using Newton's iterations. The spatial discretisation is based on a finite-element formulation using quadratic elements (P_2) and linear elements (P_1) for velocity and pressure, respectively. The numerical method has been implemented in the non-commercial software FreeFem++ (Hecht 2012) and has been previously used and validated (Chiarini *et al.* 2021*a*). For each configuration, a computational mesh that is perfectly symmetric with respect to

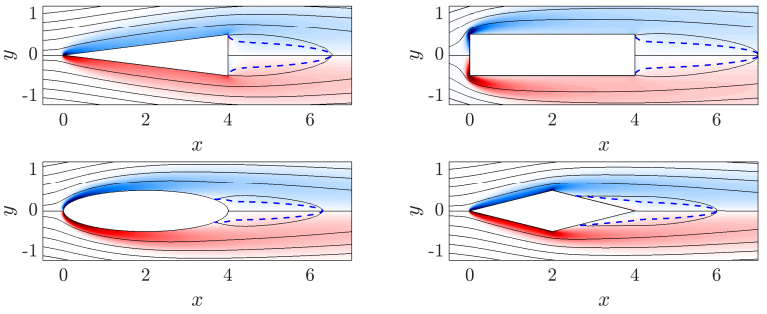

Figure 2: Base flow for the triangular (top left), rectangular (top right), elliptical (bottom left) and diamond (bottom right) cylinders for $\mathit{AR} = 4$ at $Re = Re_c$. Streamlines are plotted on top of a vorticity map ω_z, with the symmetric blue-to-red colormap ranging in $-10 \leqslant \omega_z \leqslant 10$. The blue dashed line is for $U = 0$.

the $y = 0$ axis is used, to avoid the introduction of spurious asymmetries in the flow. The number and distribution of the triangular elements has been chosen to properly refine the region around the cylinders, by paying specific attention to the near-corner regions and to the wake. The number of triangles varies between 60×10^3 and 90×10^3 depending on the body shape and aspect ratio.

The global stability analysis of the flow is carried out by solving the eigenvalue problem stemming from the Navier–Stokes equations linearised with respect to the steady base flow. The solution is obtained by the implicitly-restarted Arnoldi iterative algorithm implemented in the ARPACK package (Lehoucq *et al.* 1998). When only one eigenvalue is required, a simple shift-invert method (Saad 2011) is used.

3. Results

3.1. *Base flow*

The steady base flow for the four geometries considered in this work is shown in figure 2 for $\mathit{AR} = 4$ at a Reynolds number corresponding to the onset of the primary instability, i.e. $Re = 68.8$, $Re = 89.1$, $Re = 140.1$ and $Re = 151.1$ for the triangle, rectangle, ellipse and diamond, respectively. Being a pseudoscalar, the spatial distribution of the nonzero vorticity component $\omega_z = \partial V/\partial x - \partial U/\partial y$ is antisymmetric with respect to the $y = 0$ axis, with the largest values observed in the fore part of the cylinders. Two shear layers displaying vorticity of opposite sign separate from the rear part of each cylinder, delimiting a symmetric separation bubble. For all cases, the vorticity is maximum at the leading edge; for triangles, rectangles and diamonds the peak is localised near the sharp corners, while for ellipses, which lacks corners, the peak is smeared. A second localised and weaker peak is observed near the sharp trailing-edge corners only for triangles and rectangles. In contrast, for ellipses and diamonds, the vorticity map features a wide region with large values extending from the leading-edge stagnation point to the point where the shear layers detach. For triangles, rectangles and diamonds, the point where the boundary layer separates is geometrically fixed at the trailing-edge, leading-edge and top/bottom corners, respectively. For ellipses, instead, the separation point changes with Re and AR. On the other hand, for rectangles and triangles the streamline delimiting the separation bubble originates at the

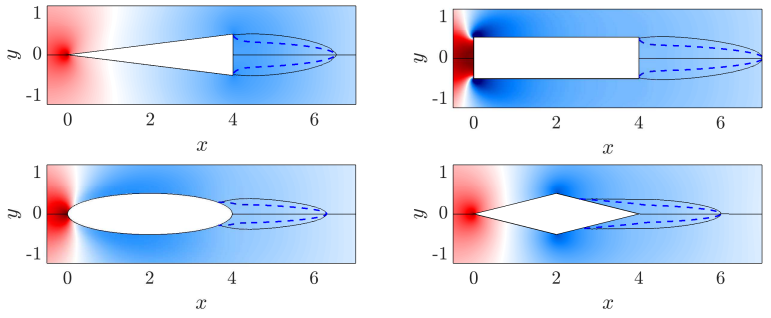

Figure 3: As figure 2, but for the pressure field P. The blue-to-red symmetric colormap ranges in $-0.5 \leqslant P \leqslant 0.5$.

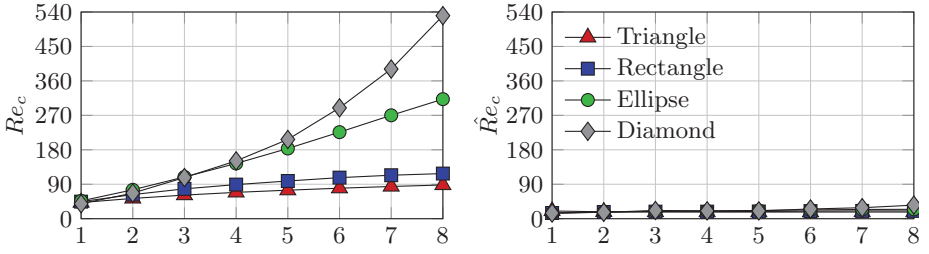

Figure 4: Dependence of Re_c (left) and $\hat{Re}_c = (U_{rev}\ell_r/\nu)|_c$ (right) on $\mathit{Æ}$ and on the cylinder geometry.

trailing-edge corners at all $\mathit{Æ}$, while for ellipses and diamonds its origin depends on Re and $\mathit{Æ}$.

Figure 3 plots pressure maps P. Unlike vorticity, pressure is symmetric with respect to the $y = 0$ axis. For all geometries, the largest values are reached at the leading-edge stagnation point, as expected, while the lowest values are observed close to the point where the shear layers separate, i.e. after the trailing-edge corners for triangles, just after the leading-edge corners for rectangles, after the top/bottom corners for diamonds and upstream of the position of maximum thickness for ellipses. As expected, the positive peak of the pressure is more intense for the rectangular and elliptic cylinders as their leading edge is blunt. The pressure distribution over the cylinder largely depends on the cylinder geometry. For triangles, starting from the leading edge and moving downstream, the pressure progressively decreases and eventually reaches its minimum at the trailing-edge corners: the pressure gradient is favourable everywhere. For rectangles, instead, the longitudinal sides feature an adverse pressure gradient as the minimum of the pressure is placed just after the leading-edge corners. The ellipses and diamonds show a different distribution, with a favourable pressure gradient in the fore part of the cylinder followed by an adverse pressure gradient in the aft part.

3.2. *Neutral curve*

The left panel of figure 4 plots how the critical Reynolds number Re_c of the primary instability, consisting in the Hopf bifurcation that produces the von Kàrmàn wake for all cases, varies with $\mathit{Æ}$ for the four shapes. For validation purpose, table 1 reports the results of our calculations for some geometries

	Present Re_c	Re_c from other references in literature
Triangle ($\mathcal{AR} = 1$)	42.1	41 (Prhashanna *et al.* 2011), 40.45 (Ng *et al.* 2016)
Rectangle ($\mathcal{AR} = 1$)	44.6	45 (Yoon *et al.* 2010), 44.7 (Park & Yang 2016)
Ellipse ($\mathcal{AR} = 1$)	46.5	46.7 (Giannetti & Luchini 2007), 46.8 (Marquet *et al.* 2008)
Ellipse ($\mathcal{AR} = 2$)	75.5	76.7 (Jackson 1987)
Diamond ($\mathcal{AR} = 1$)	39.05	39 (Yoon *et al.* 2010)

Table 1: Comparison of Re_c for some geometries with results from literature.

together with those from other references in literature and shows that they compare pretty well. The slight discrepancy for the triangular cylinder with respect to the critical values reported in literature may be probably ascribed to the different calculation methods adopted For all cases, Re_c increases with $\mathcal{AR}$: an increase of the aspect ratio leads to stabilisation regardless of the cylinder geometry. Indeed, by increasing $\mathcal{AR}$ the pockets of instability placed on the two sides of the separation bubble move downstream with respect to the point where the flow separates, so that the two shear layers that produce the instability become thicker in the instability region. This results in an increased diffusion of the shear layers and, therefore, in a weaker instability or, equivalently, in an increase of Re_c, as already observed by Chiarini *et al.* (2021*a*) for rectangles.

For triangles and rectangles, the function $Re_c(\mathcal{AR})$ increases with decreasing rate, reaching a value that is larger for the latter geometry, being $Re_c(8) \approx 90$ for triangles and $Re_c(8) \approx 120$ for rectangles. For triangles, the trend is accurately described by a power law. For triangles, this increasing trend is also related to the changes of the pressure distribution over the longitudinal sides. By plotting the pressure over a line just above or below the triangles, the favourable pressure gradient is seen to slightly decrease as $\mathcal{AR}$ increases. This contributes to a weaker blockage, highlighted by the decrease of the maximum speed above/below the trailing-edge corners, and to less intense shear layers detaching from the trailing edge, therefore resulting in a weaker instability. On the other hand, for ellipses and diamonds Re_c increases more than linearly with $\mathcal{AR}$, with diamonds showing the fastest rate of change. Quantitatively, for ellipses and diamonds Re_c respectively increases from $Re_c \approx 46.5$ and $Re_c \approx 39.1$ for $\mathcal{AR} = 1$ to $Re_c \approx 310$ and $Re_c \approx 540$ for $\mathcal{AR} = 8$. For ellipses, the curve seems to approach an oblique asymptote, that instead is not observed for diamonds. For these geometries, as for triangles, the increase of Re_c appears to be ascribed to a combination of the two effects discussed above, notwithstanding the variable position of the separation point. The superlinear growth observed for diamonds shows that the flow progressively approaches that past a flat plate as $\mathcal{AR}$ increases, since the separation point moves downstream and the vertical size of the separation bubble decreases.

4. A new scaling

Chiarini *et al.* (2021*a*) observed that, for rectangular cylinders, the absolute value of the largest reverse-flow speed within the separation bubble (U_{rev}), and the length (ℓ_r) of the bubble itself are the most important scales in the first Hopf bifurcation. They also verified that the associated Reynolds number $\hat{Re} = U_{rev}\ell_r/\nu$ predicts fairly well the onset of the instability being nearly independent on $\mathcal{AR}$. In this section, we show that this result is quite general

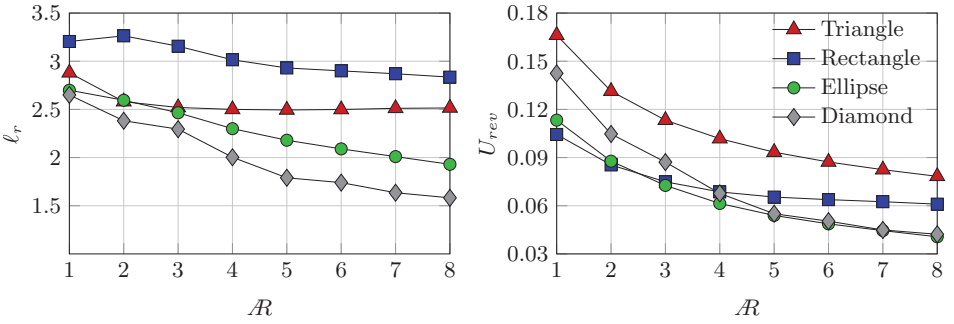

Figure 5: Effect of $\mathcal{AR}$ on the length of the separation bubble ℓ_r (left) and on magnitude of the largest reverse-flow speed U_{rev} (right).

and holds for two-dimensional cylinders of different shapes for which the primary instability corresponds to a Hopf bifurcation producing the von Kàrmàn wake.

4.1. *The reverse-flow speed*

The largest reverse-flow speed U_{rev} has a strong impact on the growth rate of the unstable mode (Hammond & Redekopp 1997). The right panel of figure 5 shows how this quantity changes with $\mathcal{AR}$ at $Re = Re_c$. In all cases, U_{rev} decreases to approach a horizontal asymptote for $\mathcal{AR} \to \infty$, because the instability mechanism becomes less intense for increasing $\mathcal{AR}$, consistently with the increase of Re_c shown in the left panel of figure 4. For small $\mathcal{AR}$, U_{rev} is maximum for triangles and minimum for rectangles: the opposite happens for ℓ_r. Interestingly, the largest decrease of $|U_{\min}|$ for large $\mathcal{AR}$ is observed for ellipses and diamonds: as $\mathcal{AR}$ ranges from $\mathcal{AR} = 1$ to $\mathcal{AR} = 8$, $|U_{\min}|$ drops by 69% and 74% for diamonds and ellipses and by about 42% and 53% for rectangles and triangles. This is consistent with the largest increase of Re_c observed for diamonds and ellipses in the left panel of figure 4.

The reverse-flow speed is relevant for two reasons: firstly, being the flow speed outside the recirculation bubble approximately constant, increasing U_{rev} increases the strength of the shear layer and therefore the amplification of the disturbances; secondly, increasing U_{rev} increases the feedback due to recirculation, the stronger the feedback the stronger the instability.

4.2. *The length of the separation bubble*

The left panel of figure 5 shows how the length of the separation bubble changes with $\mathcal{AR}$ at $Re = Re_c$. ℓ_r, defined as the distance between trailing edge of the cylinder and the stagnation point that closes the separation bubble, is found to generally decrease with $\mathcal{AR}$. This decreasing trend is explained by the same phenomena responsible for the increase of Re_c, namely the increasing diffusion of the separated shear layers and the weakening pressure gradient over the longitudinal sides. For rectangles, ℓ_r is non-monotonic for small $\mathcal{AR}$, due to the interaction of the shear layers separating from the leading-edge with the trailing-edge corners (Chiarini *et al.* 2021*a*). For triangles, ℓ_r first decreases and reaches its minimum for $\mathcal{AR} = 5$ and then slightly increases again. This (small) increase of ℓ_r is due to the slight enlargement of the streamlines at the trailing-edge corners, where the shear layers separate, associated with the progressive increase

of the boundary layer thickness. For small $\mathcal{AR}$ this effect is not appreciated, as the phenomena yielding the aforementioned decreasing trend dominate.

The size of the separation bubble is important in the onset of instability, since it is directly related to the size of the absolute instability region, the larger this region the more unstable the flow.

4.3. *The new scaling*

Figure 4 plots the evolution of $\hat{Re}_c = (U_{rev}\ell_r/\nu)|_c$ with $\mathcal{AR}$, i.e. $\hat{Re}$ evaluated at the onset of the primary instability, and compares it with changes of Re_c. For all geometries, the relative variation of $\hat{Re}_c$ with $\mathcal{AR}$ is much smaller than that of Re_c, and the values of $\hat{Re}$ at criticality collapse quite neatly on an average value of $\hat{Re}_c \approx 20$, the minimum value being $\hat{Re}_c \approx 14$ for the diamond with $\mathcal{AR} = 8$ and the largest value being $\hat{Re}_c \approx 35$ for the ellipse with $\mathcal{AR} = 1$. The collapse is not perfect, yet the relative variation is almost one order of magnitude less with the present scaling than with the standard form of the Reynolds number, whose minimum and maximum values are $Re_c \approx 39$ and $Re \approx 530$ for the diamond with $\mathcal{AR} = 1$ and $\mathcal{AR} = 8$ respectively. It is worth noting that the proposed scaling works quite well up to the highest $\mathcal{AR}$ tested for all shapes. Indeed, the value of $\hat{Re}_c$ seems to start deviating for the diamond cylinders at the largest $\mathcal{AR}$ only. This is consistent with the fact that, as observed in §3.2, in the diamond case as $\mathcal{AR}$ increases the base flow approaches that past a flat plate that displays an instability of a different nature, for which this scaling does not work.

The newly defined $\hat{Re}$, based on the magnitude of the largest reverse-flow speed U_{rev} and on the length of the separation bubble ℓ_r, is far more capable than that based on the free-stream velocity U_∞ and cylinder thickness D to predict the onset of the primary instability for the steady flow past symmetric two-dimensional bluff bodies. The implied scaling is not trivial, since ℓ_r and U_{rev} depend on $\mathcal{AR}$ quite differently for the considered geometries. It allows one to determine if the flow is linearly unstable to two-dimensional perturbations with rather good accuracy by just evaluating U_{rev} and ℓ_r and examining whether $\hat{Re}$ is larger or lower than $\hat{Re}_c \approx 20$. Computing $\hat{Re}$ only requires the knowledge of the base flow, whose computational cost is much smaller than that of a linear stability analysis.

4.4. *Other wake-related length scales*

In this section we show that the new scaling works well when other wake-related length scales are used instead of ℓ_r, provided that they are a measure of the spatial extent of the separation bubble. We keep considering U_{rev} as velocity scale and, following the idea that this instability is promoted by the base flow shear layer along the dividing streamline of the body, we consider four different length scales that are a measure of the width of the separation bubble. The new length scales are the width of both the dividing streamline ($d_{r,1}$) and the $U = 0$ line ($d_{r,2}$) at the streamwise position corresponding to the location of U_{min}, and the vertical distance between the maxima of the two structural sensitivity pockets ($d_{r,3}$) (Giannetti & Luchini 2007). Based on these length scales we define the following Reynolds numbers:

$$\hat{Re}_c^{\,d,1} = \frac{U_{rev}d_{r,1}}{\nu},\ \hat{Re}_c^{\,d,2} = \frac{U_{rev}d_{r,2}}{\nu},\ \text{and}\ \hat{Re}_c^{\,d,3} = \frac{U_{rev}d_{r,3}}{\nu}. \tag{4.1}$$

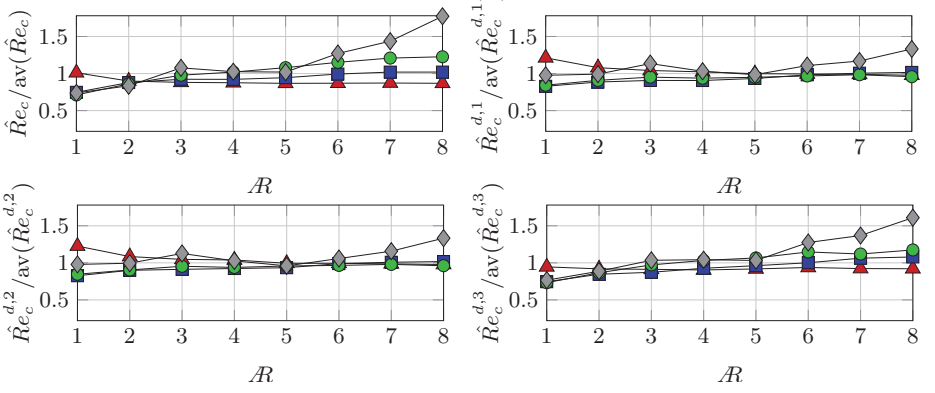

Figure 6: Dependence of the relative variation of $\hat{Re}_c$ (top left), $\hat{Re}_c^{d,1}$ (top right), $\hat{Re}_c^{d,2}$ (bottom left), $\hat{Re}_c^{d,3}$ (bottom right), as defined in equation 4.1, on $\mathcal{AR}$ and on the cylinder geometry. Symbols and colours as in figure 4.

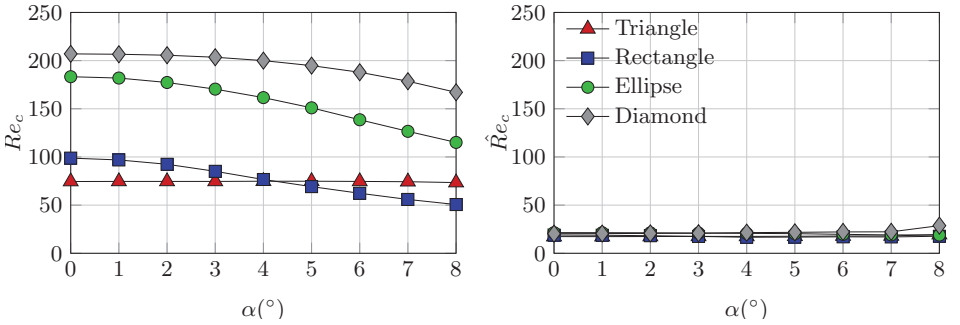

Figure 7: Dependence of Re_c (left) and $\hat{Re}_c = (U_{rev}\ell_r/\nu)|_c$ (right) on the incidence angle α and on the cylinder geometry for aspect ratio $\mathcal{AR} = 5$.

Figure 6 shows that at criticality all the new proposed Reynolds numbers collapse pretty well for all the aspect ratios and the geometries considered. For all cases the maximum variation from the average value is within 75%, that is by far smaller than the maximum variation of Re_c that is $\approx 290\%$. This is expected as all these length scales are a good measure of the spatial extent of the separation bubble, as witnessed by their dependence on both $\mathcal{AR}$ and the body shape that is qualitatively the same to what shown for ℓ_r in figure 5. Among the different proposed Reynolds numbers, those based on the width of the dividing streamline ($d_{r,1}$) and of the reverse flow region ($d_{r,2}$) show the best collapse, and their maximum relative variation is within 40%.

4.5. *Flow asymmetry*

Figure 7 deals with the robustness of the proposed scaling on asymmetries of the flow. For all the four geometries we have fixed the aspect ratio to $\mathcal{AR} = 5$ and repeated the calculations by changing the incidence angle in the range $0^\circ \leqslant \alpha \leqslant 8^\circ$. For all geometries but for the triangle, an increase of α leads to a monotonic decrease of Re_c, that goes from $Re_c = 98.8, 183.3, 207.0$ for $\alpha = 0^\circ$ to $Re_c = 50.6, 115.1, 167.1$ for $\alpha = 8^\circ$ for the rectangular, elliptical and diamond

cylinder respectively. For the triangular cylinder, instead, Re_c only marginally changes in the considered range of incidence angles, as observed by Jackson (1987) for the $\mathit{AR} = 1$ case. The right panel shows that the proposed scaling is robust to moderate asymmetries of the flow. Indeed, in this range of α the variation of $\hat{Re}_c$ is much smaller than that of Re_c and its value collapse quite well for all the body shapes: the average values is $\hat{Re}_c = 19.48$, while the minimum and maximum values are $\hat{Re}_c = 17.32$ and $\hat{Re}_c = 28.69$ for the triangle at $\alpha = 1^\circ$ and the diamond at $\alpha = 8^\circ$ respectively.

5. Conclusion

Depending on the Reynolds number, the incompressible flow past symmetric, two-dimensional bluff bodies ranges from a symmetric steady state to the turbulent regime. For this class of flows, Re is usually defined with the cross-stream size of the body D and the free-stream velocity U_∞ as $Re = U_\infty D/\nu$. When Re is large enough, i.e. $Re > Re_c$, the flow undergoes a first two-dimensional instability, the primary instability, usually corresponding to a Hopf bifurcation leading to a time-periodic flow with vortex shedding. Although the physical mechanism behind the primary Hopf instability remains the same, the numerical value of Re_c strongly varies when the cross-section and the aspect ratio of the body are varied (Jackson 1987). In this work, an alternative scaling has been proposed for the prediction of the primary Hopf instability, where the length of the separation bubble ℓ_r and the largest reverse-flow speed within it are the length and velocity scales, respectively. The appropriateness of these scales descends from their direct link to the local amplification of the unstable wave packets, and to the extension of the absolute instability region (Hammond & Redekopp 1997; Chomaz 2005). At criticality, the associated Reynolds number $\hat{Re} = U_{rev}\ell_r/\nu$ has been shown to collapse quite nicely across geometries and aspect ratios: its relative variation is one order of magnitude smaller than that of the conventional Re_c. Hence this scaling, although still not ideal, is far more appropriate for predicting the onset of the primary instability than the one based on D and U_∞. Moreover, we have shown that this scaling is robust to small asymmetries of the flow and that it works well even if other wake-related length scales are used, provided that they are a measure of the spatial extent of the separation bubble.

This observation has a significant theoretical value, inasmuch as it sheds new light on the instability mechanism leading to the von Kàrmàn vortex street. Moreover, there is practical value in the ability to readily estimate whether the two-dimensional steady flow past a bluff body is absolutely unstable to two-dimensional perturbations by avoiding a computationally expensive stability analysis.

Funding

This research received no specific grant from any funding agency, commercial or not-for-profit sectors.

Declaration of Interests

The authors report no conflict of intere

REFERENCES

Chiarini, A., Quadrio, M. & Auteri, F. 2021*a* Linear stability of the steady flow past rectangular cylinders. *Journal of Fluid Mechanics* **929**.

Chiarini, A., Quadrio, M. & Auteri, F. 2021*b* On the frequency selection mechanism of the low-Re flow around rectangular cylinders. *J. Fluid Mech.* **Accepted**.

Chomaz, J.-M. 2005 Global instabilities in spatially developing flowa: Non-normality and nonlinearity. *Annual Review of Fluid Mechanics* **37** (1), 357–392.

Giannetti, F. & Luchini, P. 2007 Structural sensitivity of the first instability of the cylinder wake. *Jounal of Fluid Mechanics* **581**, 167–197.

Hammond, D. A. & Redekopp, L. G. 1997 Global dynamics of symmetric and asymmetric wakes. *Journal of Fluid Mechanics* **331**, 231–260.

Hecht, F. 2012 New development in FreeFem++. *Journal of Numerical Mathematics* **20** (3-4), 251–266.

Hourigan, K., Thompson, M. C. & Tan, B. T. 2001 Self-sustained oscillations in flows around long blunt plates. *Journal of Fluids and Structures* **15** (3), 387–398.

Jackson, C. P. 1987 A finite-element study of the onset of vortex shedding in flow past variously shaped bodies. *Journal of Fluid Mechanics* **182**, 23–45.

Lehoucq, R.B., Sorensen, D. C. & Yang, C. 1998 *ARPACK Users' Guide: Solution of Large-Scale Eigenvalue Problems with Implicitly Restarted Arnoldi Methods*. SIAM.

Marquet, O., Sipp, D. & Jacquin, L. 2008 Sensitivity analysis and passive control of cylinder flow. *Journal of Fluid Mechanics* **615**, 221–252.

Mat Ali, Mohamed Sukri, Doolan, Con J. & Wheatley, Vincent 2011 Low Reynolds number flow over a square cylinder with a splitter plate. *Physics of Fluids* **23** (3), 033602.

Monkewitz, P. A., Huerre, P. & Chomaz, J.-M. 1993 Global linear stability analysis of weakly non-parallel shear flows. *Journal of Fluid Mechanics* **251**, 1–20.

Ng, Zhi Y., Vo, Tony, Hussam, Wisam K. & Sheard, Gregory J. 2016 Two-dimensional wake dynamics behind cylinders with triangular cross-section under incidence angle variation. *Journal of Fluids and Structures* **63**, 302–324.

Noack, B. R. & Eckelmann, H. 1994 A global stability analysis of the steady and periodic cylinder wake. *Journal of Fluid Mechanics* **270**, 297–330.

Okajima, A. 1982 Strouhal numbers of rectangular cylinders. *Journal of Fluid Mechanics* **123**, 379–398.

Park, D. & Yang, K.-S. 2016 Flow instabilities in the wake of a rounded square cylinder. *Journal of Fluid Mechanics* **793**, 915–932.

Pope, S.B. 2000 *Turbulent Flows*. Cambridge University Press, Cambridge.

Prhashanna, A., Sahu, Akhilesh K. & Chhabra, R. P. 2011 Flow of power-law fluids past an equilateral triangular cylinder: Momentum and heat transfer characteristics. *International Journal of Thermal Sciences* **50** (10), 2027–2041.

Provansal, M., Mathis, C. & Boyer, L. 1987 Bénard-von Kármán instability: Transient and forced regimes. *J Fluid Mech* **182**, 1–22.

Saad, Y 2011 *Numerical Methods for Large Eigenvalue Problems*. Philadelphia: Society for Industrial and Applied Mathematics.

Thompson, M.C., Radi, A., Rao, A., Sheridan, J. & Hourigan, K. 2014 Low-Reynolds-number wakes of elliptical cylinders: From the circular cylinder to the normal flat plate. *Journal of Fluid Mechanics* **751**, 570–600.

Williamson, C H K 1996 Vortex Dynamics in the Cylinder Wake. *Annual Review of Fluid Mechanics* **28** (1), 477–539.

Yoon, D.-H., Yang, K.-S. & Choi, C.-B. 2010 Flow past a square cylinder with an angle of incidence. *Physics of Fluids* **22** (4), 043603.